TRENDS IN SCIENCES 2026; 23(10): 13505
https://doi.org/10.48048/tis.2026.13505 RESEARCH ARTICLE

Hibiscus sabdariffa Extract-Based, Green-Synthesized Ag-PANI Nanocomposite for Antibacterial, Antioxidant, and Anticancer Activities

Rusul Ali Al-Masaoodi[1], Muhammad Riyadh Alkenany[2,*], Ahmed A. Abdul-Azeez AL-Safar[1] and Noor Ali Abdul Al lmmah Al Salman[3]

[1]*Department of Medical Biochemistry, Faculty of Medical Applied Sciences, University of Kerbala, Karbala 56001, Iraq*
[2]*Department of Medical Physics, Faculty of Medical Applied Sciences, University of Kerbala, Kerbala 56001, Iraq*
[3]*Department of Physiology, Biochemistry and Pharmacology College of Veterinary Medicine, University of Karbala, Karbala 56001, Iraq*

([*]Corresponding author's e-mail: Muhammad.r@uokerbala.edu.iq)

Received: 30 January 2026, Revised: 25 March 2026, Accepted: 5 April 2026, Published: 5 May 2026

Abstract

Multifunctional nanocomposites with anticancer, antioxidant, and antibacterial activities are increasingly needed to address cancer progression, oxidative stress, and microbial resistance using biocompatible and eco-friendly materials. In this study, a green-synthesized Ag-PANI nanocomposite was successfully prepared using *Hibiscus sabdariffa* extract and evaluated for its physicochemical characteristics and biological performance. Structural and morphological analyses confirmed the successful formation of the nanocomposite and the incorporation of Ag nanoparticles within the PANI matrix. The Ag-PANI nanocomposite exhibited improved colloidal behavior, with a reduced hydrodynamic size distribution of about 500 - 600 nm and a positive zeta potential of approximately +22 mV, indicating enhanced dispersion stability compared with pure Ag nanoparticles and pristine PANI. In vitro cytotoxicity against breast cancer cells revealed a clear concentration-dependent reduction in cell viability, with an estimated IC_{50} in the intermediate concentration range. The nanocomposite also showed notable antioxidant activity, with effective radical scavenging performance in DPPH, H_2O_2, hydroxyl, and superoxide assays. In addition, it demonstrated strong antibacterial activity against *Escherichia coli* and *Staphylococcus aureus*, with maximum inhibition zones of 24.0 ± 0.91 and 21.0 ± 0.73 mm, respectively, at 1250 µg/mL. These findings indicate that the green-synthesized Ag-PANI nanocomposite is a stable and promising multifunctional platform for anticancer, antioxidant, and antibacterial biomedical applications.

Keywords: Ag-PANI nanocomposite, Green synthesis, *Hibiscus sabdariffa*, Breast cancer, Antioxidant activity, Antibacterial activity

Introduction

Cancer is still among the gravest health problems in the world and one of the major causes of death on the global level with a significant impact on health care systems [1-3]. Traditional methods of cancer treatment, such as chemotherapy and radiotherapy, usually have serious side effects, low specificity to cancer cells, and the emergence of drug resistance [4,5]. Such drawbacks have led to extensive studies to find alternative treatment methods that will be more effective and selective, as well as biocompatible [6,7].

Nanotechnology provides a promising platform in the field of biomedical research, especially in cancer treatment and diagnosis owing to the special physicochemical characteristics of nanomaterials which comprise high surface area, size manipulation, and greater interactions with biological systems [8-10]. The cellular uptake can be enhanced by nanomaterials which

enhances therapeutic efficacy and decreases the toxicity of normal cells relative to traditional bulk materials [11,12]. Consequently, nanostructured systems have received growing interests in anticancer, antioxidant and antimicrobial applications [13,14].

One of the widely studied nanomaterials is the silver-based nanostructures, due to their extraordinary biological functionality, such as high anticancer and antibacterial properties [15-17]. Silver nanoparticles have been identified to cause cytotoxicity in cancer cells in several ways including the production of reactive oxygen species (ROS), mitochondrial dysfunction and DNA damage and possess relatively low toxicity to normal cells at maximized concentrations [18-20]. Nevertheless, aggregation propensity of silver nanoparticles and their low stability can diminish their usefulness in biomedical use [21].

Investigations into conductors of polymers especially polyaniline (PANI) have resulted in a lot of attention due to their high electrical conductivity, stability in the environment, facile production and bio compensation of the polymer [22-24]. The informative polymer network of PANI and chemical stability have been used extensively in biomedical applications, such as drug delivery, biosensors, and tissue engineering because these materials are conductive polymer networks, and because of their chemical stability [25]. It is possible to create hybrid nanocomposites with enhanced physicochemical and biological characteristics by including metallic nanoparticles in the PANI matrix. The primary role of PANI in these systems is to prevent aggregation of nanoparticles to form stable nanoparticles and to amplify the electron transfer and surface interaction. The properties may be used to a great extent to enhance the biological performance of metal-polymer nanocomposites, such as anticancer, antioxidant, and antibacterial functions in nanoparticles under the synergistic effects of the metallic nanoparticles and the conductive polymer framework [26].

However, several studies have reported that polyaniline exhibits relatively low cytotoxicity at controlled concentrations and demonstrates acceptable biocompatibility in biomedical systems, particularly when incorporated into polymer-metal nanocomposites, where the polymer matrix can regulate nanoparticle dispersion and reduce potential toxicity effects [27].

Synthesis of Ag-PANI nanocomposites has proved to be a viable approach in integrating the excellent biological action of silver nanoparticles with the mechanical properties of stability and conductivity of polyaniline [28,29]. These hybrid nanocomposites have increased cytotoxic cancer killing in cancer cells, increased antioxidant radical scavenging and enhanced antibacterial activity because of the synergistic action of metal nanoparticles and polymeric networks [30-33]. These are synergistic effects that provide Ag-PANI nanocomposites as promising candidates in multifunctional biomedical applications.

Green synthesis strategies have become a popular topic in the last few years due to their environmentally friendly substitutes of the traditional chemical and physical synthesis techniques [34,35]. Plant extracts are natural reducing and stabilizing agents, and toxic chemicals are not required and instead increase the biocompatibility of the nanomaterials formed [36]. The reduction of silver ions using Hibiscus sabdariffa extract tea contains bioactive compounds including polyphenols, flavonoids, anthocyanins, and organic acids, which may be effectively used to stabilize the nanoparticles formed [37]. Besides, these phytochemicals are also characterized by their inherent antioxidant, anticancer, and antimicrobial effects, which also add to the biological functionality of the produced nanocomposites [38].

The novelty of the current work consists in the synthesis strategy of green synthesis and a thorough biological analysis. Natural reducing and stabilizing agent *Hibiscus sabdariffa* extract was used to prepare the Ag-PANI nanocomposite and this offers an eco-friendly process of preparing the nanocomposite. Moreover, this synthesized material was assessed systematically regarding anticancer, antioxidant, and antibacterial properties, which demonstrate its further use as a multifunctional nanomaterial in biomedical uses.

Nevertheless, although Ag-PANI nanocomposites have a promising biological property as reported in the literature, little attention has been drawn to the use of the nanocomposites in many biomedical scenarios especially in multifunctional applications even though most of the past research has mainly considered their antibacterial or electrochemical uses, especially when synthesized in environmentally friendly processes. The

Ag-PANI nanocomposite in the given work was produced through the green synthesis approach with the help of *Hibiscus sabdariffa* extract that naturally presents reducing and stabilizing agents. This will reduce the utilization of toxic chemicals as well as will add new bio-active compounds into the composite that could be beneficial in improving the biological performance of the composite. In addition, the current research analytically examines the anticancer, antioxidant, as well as antibacterial properties of the Ag-PANI nanocomposite, which would have an opportunity to serve as a versatile nanomaterial in biomedical practice.

Materials and methods

Material

Silver precursor ($AgNO_3$ 99.9% purity, Sigma-Aldrich) was the raw material in the synthesis of silver nanoparticles. Preparation of polyaniline matrix was done using aniline monomer ($C_6H_5NH_2$, 99% Merck), which was distilled under reduced pressure before use to eliminate oxidative impurities. The oxidizing agent in oxidizing aniline polymerization was ammonium persulfate (APS, $(NH_4)_2S_2O_8$, 98%, Merck). The acidic medium needed to carry out the polymerization process was the hydrochloric acid (HCl, 37%, Merck).

The natural reducing and stabilizing agent of green synthesis route was the dried calyces of *Hibiscus sabdariffa*. The plant material was acquired in a local market, but it was carefully washed using distilled water and then dried at room temperature followed by storage before extract preparation. All the solutions were prepared using deionized water in the entire course of the experiment.

Green synthesis of Ag-PANI nanocomposite

The Ag-PANI nanocomposite was synthesized through a green oxidative polymerization approach using *Hibiscus sabdariffa* extract as a natural reducing and stabilizing agent, as illustrated in **Figure 1**. *Hibiscus sabdariffa* was selected due to its high content of bioactive phytochemicals, including polyphenols, flavonoids, and organic acids, which are known to facilitate the reduction of metal ions and stabilize the formed nanoparticles during green synthesis. These phytochemicals may also contribute to the enhanced biological activity of the resulting nanocomposite. Although the phytochemical content of the extract was not quantitatively determined in this study, previous reports indicate that *Hibiscus sabdariffa* extract contains significant amounts of these compounds, which can effectively participate in the reduction and stabilization of metal nanoparticles.

Briefly, dried *Hibiscus sabdariffa* calyces (10 g) were thoroughly washed with distilled water and boiled in 100 mL of deionized water at 80 °C. After cooling to room temperature, the extract was filtered to obtain a clear plant extract [39]. A 0.01 M $AgNO_3$ solution was prepared by dissolving 0.1699 g of $AgNO_3$ in 100 mL of deionized water. Subsequently, 20 mL of the plant extract was gradually added to 50 mL of the $AgNO_3$ solution under continuous stirring at room temperature for 30 min to promote the reduction of Ag^+ ions and the formation of Ag nanoparticles.

After the Ag nanoparticles were formed 1.0 mL aniline monomer was added to the reaction mixture of 50 mL of 1.0 M HCl as the acidic medium. The oxidative polymerization process of aniline was triggered by slowly adding 0.228 g ammonium persulfate (APS) dissolved in 50 mL of deionized water at 0 - 5 °C. Continuous stirring of the reaction mixture was done over a period of 6 h in order to achieve full polymerization. The precipitate resulting was filtrated to acquire the dark-green precipitate, and several washes of the precipitate using deionized water and ethanol were made to eliminate unreacted species, then the precipitate was dried in 60 °C over a period of 12 h to give the Ag-PANI nanocomposite powder

In this system, polyaniline mainly functions as a stabilizing polymer matrix that supports the dispersion of silver nanoparticles and prevents their aggregation. Although aniline contains amine groups that may weakly participate in reduction reactions, the primary reduction of Ag^+ ions in this green synthesis process is mainly driven by phytochemicals present in the *Hibiscus sabdariffa* extract. The reduction process was carried out at the natural pH of the plant extract without additional pH adjustment.

Figure 1 Schematic illustration of the green synthesis of the Ag-PANI nanocomposite using *Hibiscus sabdariffa* extract, showing the sequential reduction of Ag^+ ions to Ag nanoparticles followed by oxidative polymerization of aniline to form the PANI matrix.

Cell culture

MCF-7 human breast cancer cells were used to assess the anticancer properties of the Ag-PANI nanocomposite that had been synthesized. The cells were grown in Dulbecco Modified Eagle Medium (DMEM) with 10% fetal bovine serum (FBS) and 1% penicillin streptococci to avoid contamination by microorganisms and to supply the cell with nutrients required to grow [39]. Standard cell culture conditions were used to keep the cell cultures in humidified incubator at 37 °C and 5% CO_2. The subculture with the trypsin-EDTA followed by seeding the cells into the relevant culture plates at a specific density in advance was done to ensure that the cells attached and stabilized properly before the biological assays. Cell morphology and confluence were regularly measured by the use of inverted optical microscope and the culture media were periodically changed to ascertain healthy and even cell proliferation prior to the treatment with the nanocomposite.

Cytotoxicity test

The cytotoxic activity of the synthesized Ag-PANI nanocomposite was evaluated using the MTT assay, which is based on the metabolic reduction of tetrazolium salt into insoluble formazan crystals by viable cells. Cells were seeded in 96-well culture plates at a density of approximately 1×10^4 cells per well and allowed to adhere overnight under standard incubation conditions (37 °C, 5% CO_2). After reaching appropriate confluence, the cells were treated with different concentrations of the Ag-PANI nanocomposite and incubated for a specified period to evaluate dose-dependent cytotoxicity. Then, MTT solution was added to each well and further incubated the plates to enable the formazan crystals to be formed. The medium was then removed with care and the crystals formed were then dissolved in an appropriate solvent. Absorbance of the dissolved formazan was taken by measuring at the wavelength of 570 nm with a microplate reader and cell viability was computed when compared to untreated control cells. The values obtained were put in terms of percentage cell viability, which gives a quantitative measure of cytotoxic effect of the nanocomposite [40,41].

Antioxidant activity

The antioxidant activity of the Ag-PANI nanocomposite was evaluated using several conventional spectroscopic assays to determine its ability to scavenge different free radicals. Four major tests were performed: The DPPH radical assay,

hydrogen peroxide (H_2O_2) scavenging assay, hydroxyl radical (•OH) assay, and superoxide anion ($^{-}O_2$) assay [42]. All measurements were conducted at room temperature (25 ± 2 °C) using a UV-Vis spectrophotometer (Shimadzu UV-1900).

For the DPPH assay, a 0.1 mM DPPH solution was prepared in ethanol. One mL of this solution was mixed with 1 mL of the Ag-PANI nanocomposite suspension (1 mg/mL). The mixture was kept in the dark for 45 min and the absorbance was measured at 517 nm. The percentage of radical scavenging activity was calculated using the following equation [43]:

$$\text{Inhibition } (\%) = \frac{A_0 - A_S}{A_0} \times 100 \quad (1)$$

where, A_s represents the absorbance of the sample solution containing the Ag-PANI nanocomposite, and A_o represents the absorbance of the control (blank) solution without the nanocomposite.

In hydrogen peroxide (H_2O_2) test, a 40 mM solution of H_2O_2 was prepared in phosphate buffer (pH = 7.4). One mL of the sample solution was combined with 1 mL of this solution and left to incubate over a period of 15 min. Absorbance was subsequently recorded in 230 nm.

For the hydroxyl radical (•OH) assay, the Fenton reaction system was prepared by mixing 1 mL of $FeSO_4$ (1 mM), one mL of H_2O_2 (1 mM), and 1 mL of the sample solution. After 20 min of incubation, the absorbance was recorded at 532 nm.

The superoxide anion ($^{-}O_2$) scavenging assay was performed using a radical generation system consisting of nicotinamide adenine dinucleotide (NADH), nitro blue tetrazolium (NBT), and phenazine methosulfate (PMS). One mL of NADH (156 µM) was mixed with 1 mL of NBT (50 µM) and 1 mL of PMS (10 µM), followed by the addition of 1 mL of the sample solution. After 5 min of incubation, the absorbance was measured at 560 nm.

Experiments were conducted three times and in each case the results were reported in the form of mean and standard deviation (mean ± SD). The antioxidant effect of the samples was measured against vitamin C as a sample antioxidant [44].

Agar well diffusion

Gram-negative *Escherichia coli* and Gram-positive *Staphylococcus aureus* bacteria were run to ascertain the antibacterial activity of the Ag-PANI nanocomposite using the agar well diffusion method. Agar plates of Mueller-Hinton were inoculated with freshly prepared bacterial suspensions and Gram-positive bacterial lawns were obtained. Wells of 6 mm diameter aseptic punches were made on the agar. The concentrations of Ag-PANI nanocomposites (250, 500, 750, 1,000 and 1,250 µg/mL) were prepared and 100 µL of each solution put in its corresponding wells. Both plates were incubated at 37 °C of the incubation time 24 h and the antibacterial activity was then measured in millimeters of the inhibition zones. A standard antibiotic (ciprofloxacin, 10 µg) was used as a positive control to compare the antibacterial activity of the Ag-PANI nanocomposite.

Characterization

Multiple analytical techniques were employed to characterize the synthesized Ag-PANI nanocomposite in terms of its structural, morphological, and physicochemical properties. X-ray diffraction (XRD) analysis was carried out using an XRD diffractometer (Bruker D8 Advance, Germany) with Cu Kα radiation (λ = 1.5406 Å) over an appropriate 2θ range to determine the crystalline structure and phase composition. The surface morphology and particle distribution were examined using field-emission scanning electron microscopy (FESEM, TESCAN MIRA3, Czech Republic). Elemental composition and distribution were analyzed using energy-dispersive X-ray spectroscopy (EDX) attached to the FESEM system. Fourier transform infrared spectroscopy (FTIR, Shimadzu IRTracer-100, Japan) was used to identify the functional groups and possible chemical interactions between the polyaniline matrix and silver nanoparticles in the range of 4,000 - 400 cm^{-1}. In addition, the optical properties of the samples were investigated using UV-Vis spectroscopy (Shimadzu UV-1900, Japan) within the wavelength range of 200 - 800 nm.

Statistical analysis

The differences between the experimental values were statistically analyzed to identify the importance of the differences by applying SPSS software, that is, a 1-

way ANOVA. The results of the final values were in the form of Mean ± SD. Statistically significant results were taken to be $p < 0.05$ [45].

Results and discussion

X-ray diffraction analysis

Figure 2 presents the X-ray diffraction (XRD) patterns of pure Ag nanoparticles, pristine polyaniline (PANI), and the Ag-PANI nanocomposite. The diffraction peaks observed at 2θ values of 38.1°, 44.3°, 64.5°, and 77.4° correspond to the (111), (200), (220), and (311) crystallographic planes of face-centered cubic (fcc) metallic silver, respectively. These reflections confirm the successful formation of crystalline Ag nanoparticles. The sharp peaks indicate the well-defined crystalline nature of the Ag phase.

In contrast, pristine PANI exhibits a broad diffraction band centered around 2θ ≈ 20 - 25°, which is characteristic of the semi-crystalline nature of polyaniline. This feature arises from the periodic arrangement of polymer chains combined with the presence of amorphous regions within the polymer structure. Such diffraction behavior is typical for polyaniline synthesized via oxidative polymerization and reflects the limited long-range structural order of the polymer matrix [46].

In the case of Ag-PANI nanocomposite, both the coexistence of the 2 components is clear in the diffraction pattern. The typical reflections of metallic Ag have been maintained in the polymer matrix which proves the effective entrapment of Ag nanoparticles in a framework of PANI. The slight expansion of the Ag diffraction peaks is an indication that the crystallite size is smaller, and the lattice is possibly distorted due to interfaces between Ag nanoparticles and PANI polymer chains. These are effects that are usually seen when nanoparticles are trapped in a polymer framework, and it is an indicator that Ag is homogeneously dispersed throughout the polymer network and does not imply simple physical mixing [47].

$$D = \frac{0.9\lambda}{\beta \cos \theta}$$

where, D is the crystallite size, λ is the X-ray wavelength (1.5406 Å), β is the full width at half maximum (FWHM) of the diffraction peak, and θ is the Bragg angle. The calculated crystallite size was found to be approximately 28 nm, which is in good agreement with the particle size range observed in the FESEM images.

Furthermore, the slight shift observed in the PANI diffraction band in the Ag-PANI nanocomposite compared with pristine PANI can be attributed to structural interactions between Ag nanoparticles and the polymer chains. The incorporation of Ag nanoparticles may induce minor changes in the interchain spacing and local structural arrangement of PANI, resulting in the observed peak shift in the XRD pattern. Overall, the coexistence of crystalline Ag and semi-crystalline PANI confirms the successful formation of the hybrid Ag-PANI nanocomposite structure. Such structural integration can enhance charge-transfer efficiency and surface reactivity, which are important factors contributing to the improved biological performance of the nanocomposite in anticancer and antibacterial applications [48].

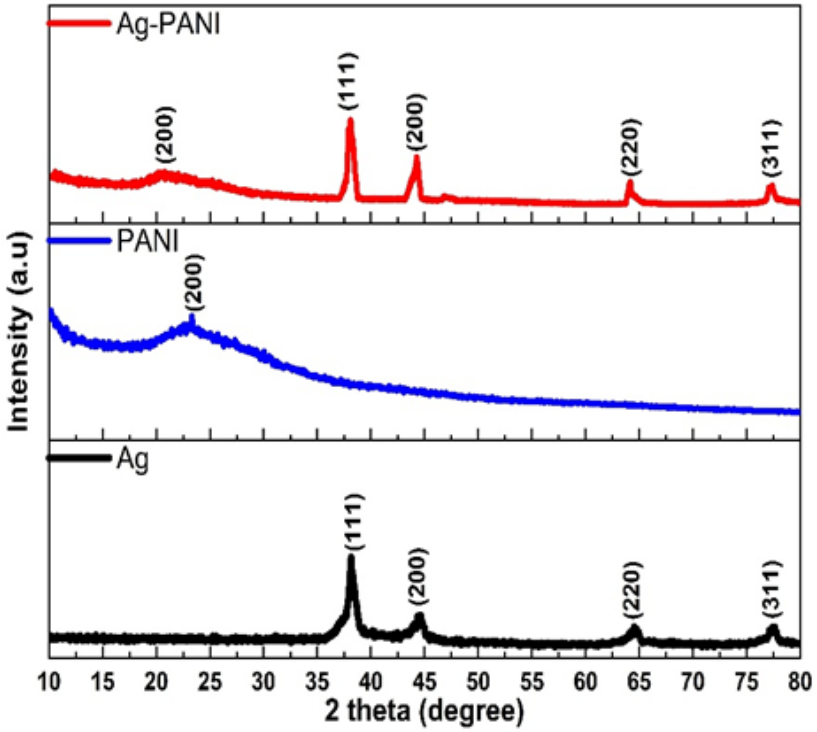

Figure 2 XRD patterns of Ag nanoparticles, pristine PANI, and the Ag–PANI nanocomposite recorded using Cu Kα radiation (λ = 1.5406 Å) over a 2θ range of 20° - 80°.

FESEM and EDX analysis

Figure 3 presents the FESEM images together with the corresponding EDX spectra of Ag nanoparticles, pristine polyaniline (PANI), and the Ag-PANI nanocomposite. The FESEM image of Ag nanoparticles shows that there is a specific level of agglomeration between the quasi-spherical particles with the particle sizes of about 25 - 45 nm. The EDX analysis shows that the dominant element is Ag (Ag 72 wt%), and oxygen (O 28 wt%) could be the result of surface adsorption or biomolecules of the *Hibiscus sabdariffa* extract that was used in the process of green synthesis. No typical Ag_2O diffraction peaks in the XRD pattern indicates that oxygen found is largely related to the biomolecule present on the surface as opposed to the development of silver oxide.

In contrast, pristine PANI exhibits a porous and interconnected polymeric morphology composed of irregular clusters and fibrous-like structures. The EDX spectrum is mainly dominated by carbon (C 73 wt%) and nitrogen (N 16 wt%), with smaller contributions from oxygen (O 8 wt%) and chlorine (Cl 3 wt%). The presence of chlorine confirms the formation of acid doped PANI because of polymerization in the HCl medium.

In the case of Ag-PANI nanocomposite, FESEM image reveals that the Ag nanoparticles are well spread and integrated into the porous PANI structure with less aggregation. It is approximated that the size of the particle, within the polymer matrix, is about 20 - 35 nm, which implies that the polymer network helps in the stable distribution of the Ag nanoparticles and prevents their growth. The EDX spectrum confirms the presence of Ag, C, N, O, and Cl with approximate compositions of Ag (60 wt%), C (25 wt%), N (8 wt%), O (5 wt%), and Cl (2 wt%). It should be noted that the elemental percentages obtained from EDX analysis represent the surface composition of the material. Therefore, the reported Ag content reflects the approximate surface distribution within the Ag-PANI nanocomposite rather than an exact bulk loading value. The decrease in Ag content compared with pure Ag nanoparticles, together with the appearance of C and N signals, confirms the successful incorporation of Ag within the PANI matrix. These observations are further supported by FTIR results, where slight shifts in the characteristic bands of PANI indicate interactions between Ag nanoparticles and nitrogen-containing functional groups of the polymer chains.

Overall, these results confirm the formation of a structurally integrated Ag-PANI nanocomposite in which nanoscale Ag particles are uniformly distributed within the doped PANI framework, providing a large interfacial surface area that may contribute to enhanced biological activity [49].

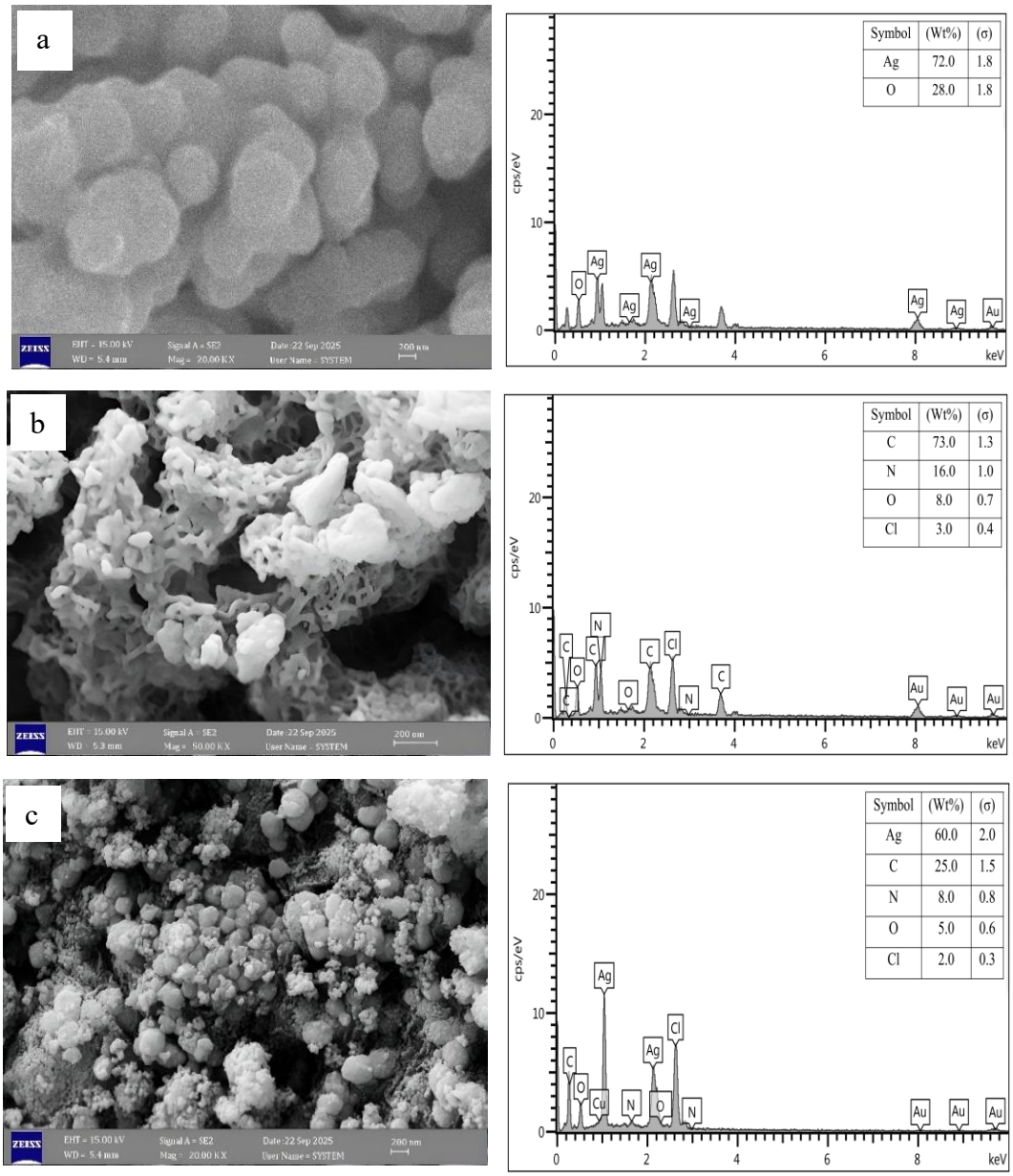

Figure 3 FESEM images and corresponding EDX spectra of (a) Ag nanoparticles, (b) pristine PANI, and (c) the Ag-PANI nanocomposite showing morphology and elemental composition.

UV-Vis optical analysis

Figure 4 presents the UV-Vis absorption spectra of Ag nanoparticles, pristine polyaniline (PANI), and the Ag-PANI nanocomposite. The spectrum of Ag nanoparticles shows a broad absorption band centered at approximately 520 - 540 nm, which corresponds to the localized surface plasmon resonance (LSPR) of metallic silver nanoparticles. The broad nature of this band suggests the formation of polydisperse nanoparticles with a certain degree of aggregation. This observation is consistent with the FESEM images, and the particle size distribution obtained from PSA analysis, both of which indicate the presence of particles with variable sizes and partial agglomeration [50].

Pristine PANI exhibits characteristic absorption features in the UV-visible region. The band observed around 320 - 350 nm is attributed to the π–π* transition of the benzenoid rings within the polymer backbone,

while the broader band in the range of 480 - 520 nm corresponds to polaron–bipolaron transitions associated with the doped conductive state of polyaniline. These spectral features confirm the successful formation of electrically conductive PANI.

In the example of Ag-PANI nanocomposite, spectral changes can be observed with respect to the single components. The typical plasmon band of Ag becomes displaced towards shorter wavelength towards an area of around 400 nm which means that there are smaller and better dispersed Ag nanoparticles that are stabilized in the PANI matrix. Such a change implies that polymer skeleton inhibits the growth of nanoparticles and enhances their dispersion. In addition, the characteristic absorption bands of PANI remain visible in the composite spectrum, confirming the successful incorporation of PANI into the Ag-PANI nanostructure. The enhanced absorption intensity observed in the visible region (400 - 700 nm) further indicates strong electronic interactions and efficient charge transfer between Ag nanoparticles and the conjugated polymer chains [51].

The extended optical absorption of the Ag-PANI nanocomposite in the visible region may enhance light-matter interaction and could potentially contribute to photothermal or photodynamic effects in biomedical applications. However, the photothermal performance was not experimentally evaluated in the present study and therefore requires further investigation [52].

The broad plasmon band observed for Ag nanoparticles is also consistent with the PSA results, which indicate a relatively wide particle size distribution and partial aggregation in the colloidal system.

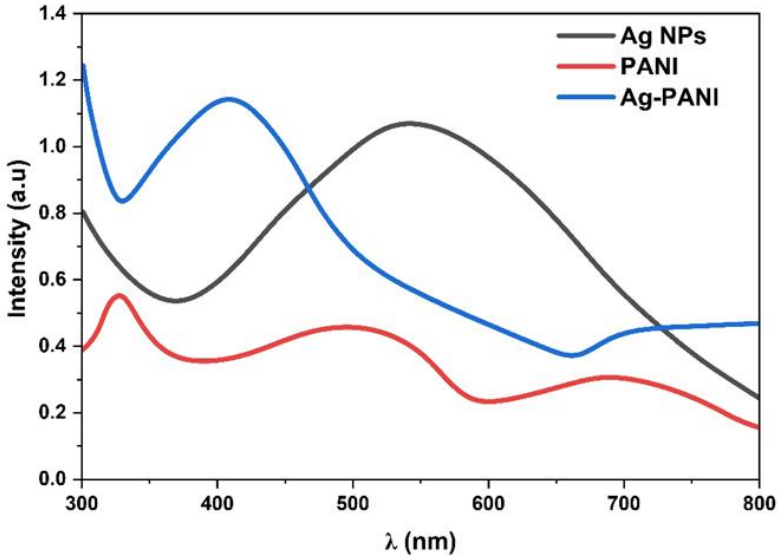

Figure 4 UV-Vis absorption spectra of Ag nanoparticles, pristine PANI, and the Ag-PANI nanocomposite recorded in the wavelength range of 200 - 800 nm.

FTIR analysis

Figure 5 shows the FTIR spectra of Ag nanoparticles, pristine polyaniline (PANI), and the Ag-PANI nanocomposite. The spectrum of Ag nanoparticles exhibits a broad absorption band around 3,371 cm^{-1}, which is attributed to O–H stretching vibrations originating from adsorbed moisture or surface hydroxyl groups formed during the green synthesis process. A band near 1,737 cm^{-1} is associated with surface-bound oxygenated species, while the low-wavenumber band around 661 cm^{-1} corresponds to Ag–O or Ag lattice vibrations, confirming the formation of nanoscale silver nanoparticles [53].

The FTIR spectrum of pristine PANI shows several characteristic bands that confirm the polymer structure. The bands observed at 2,866 and 2,641 cm^{-1} correspond to C–H stretching vibrations of the polymer backbone. The band at 1,533 cm^{-1} is attributed to the quinoid ring stretching vibration, while the band around ~1,480 - 1,500 cm^{-1} is associated with the benzenoid ring vibration, indicating the coexistence of different oxidation states of polyaniline. In addition, bands

observed in the region of approximately 1,000 - 1,250 cm^{-1} are assigned to C–N stretching vibrations of the PANI backbone, while the band near ~906 cm^{-1} corresponds to out-of-plane C–H bending, which is characteristic of doped polyaniline [54].

Compared with pristine PANI, noticeable spectral changes are observed in the Ag-PANI nanocomposite. A broad band around 3,115 cm^{-1} corresponding to N–H stretching vibrations becomes broadened and slightly shifted, suggesting interactions between Ag nanoparticles and nitrogen-containing functional groups in the PANI chains. The characteristic quinoid and benzenoid bands at approximately 1,552 and 1,349 - 1,218 cm^{-1} are preserved in the composite but exhibit slight shifts and intensity variations, indicating strong interfacial interactions and possible coordination between Ag nanoparticles and the polymer matrix. Additionally, the appearance or enhancement of bands around ~836 cm^{-1} further supports the successful incorporation of Ag nanoparticles within the PANI framework.

In general, it is possible to conclude that FTIR shows that the basic chemical structure of PANI remains intact after the composite formation. Nevertheless, the shifted bands and variation in the intensity is a clear indication of the interaction between Ag nanoparticles and nitrogen functional groups of the polymer chains. The interactions also lead to the structural stability of Ag-PANI nanocomposite and can be significant in improving functional and biological properties of the nanocomposite [55].

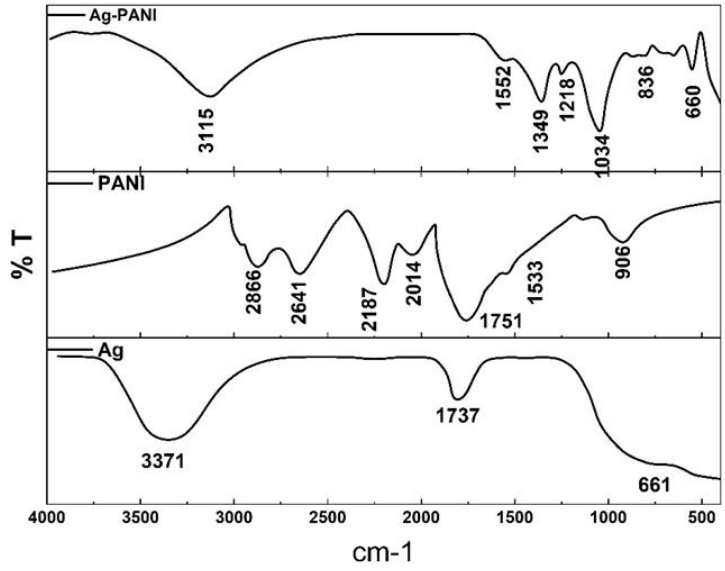

Figure 5 FTIR spectra of Ag nanoparticles, pristine PANI, and the Ag-PANI nanocomposite measured in the wavenumber range of 4,000 - 400 cm^{-1}.

Particle size distribution and zeta potential analysis

Figures 6(a) and **6(b)** depict the hydrodynamic size distribution and zeta potential of Ag nanoparticles, pure PANI and Ag-PANI nanocomposite, respectively. As **Figure 6(a)** depicts, Ag nanoparticles show a rather wide size distribution with the major population at around 650-700 nm, representing the formation of agglomerates in aqueous suspension, and in keeping with the high surface energy and partial aggregation disposition of free Ag nanoparticles in liquid.

Pristine PANI exhibits a skewed particle size distribution with a preeminent hydrodynamic diameter of 600 - 750 nm, which could be explained by the polymeric character of PANI and the assemblage of the chain in suspension. This is characteristic of conductive polymer suspended in aqueous medium and indicative of the existence of polymer domains interconnected instead of free nanoparticles [56].

On the contrary, Ag-PANI nanocomposite has a relatively smaller and shifted size distribution with the major peak at around 500 - 600 nm. The decreasing size in hydrodynamics suggests that the dispersion stability

of the Ag nanoparticles incorporated into the PANI matrix is enhanced and unwanted aggregation in the solution is prevented. This tendency indicates the presence of close interfacial interactions between Ag and PANI, which result in smaller and more stable compound entities in suspension.

The zeta potential values of **Figure 6(b)** also imply this. The zeta potentials of the Ag nanoparticles, pristine PANI and Ag-PANI nanocomposite are around +21, +18, and +22 mV respectively. The higher positive zeta potential of Ag-PANI nanocomposite indicates better colloidal stability of the particle in relation to the components, which can be attributed to the reversal of the surface charge of the Ag nanoparticles and protonated PANI chains. The quantitative parameter of this change in the magnitude of zeta potential of the nanocomposite, is more strength of electrostatic repulsion in the interaction of the particles and consequently reduces aggregation and increases the stability of the suspension [57].

The measured zeta potential value of +22 mV indicates moderate colloidal stability of the Ag-PANI nanocomposite dispersion. Although values above ±30 mV are generally considered highly stable, values within the range of ±20 - 30 mV still suggest reasonable electrostatic stabilization of nanoparticles in suspension.

In general, the analysis of the DLS, and zeta potential indicates that Ag-PANI nanocomposite has better dispersion features and an increased colloidal stability in aqueous conditions than the pure Ag nanoparticles and PANI. This improved stability is an essential consideration to biological applications, which enables easier interface with cells and bacteria and leads to predictable anticancer and antibacterial behavior

The positive surface charge observed for Ag, PANI, and the Ag-PANI nanocomposite can be attributed to protonated amine groups ($–NH_3^+$) present in the polyaniline chains under acidic conditions, which contribute to the overall positive zeta potential of the system.

The larger particle size obtained from DLS measurements compared with FESEM observations can be attributed to the hydrodynamic diameter measured in solution. DLS analysis reflects the effective size of nanoparticles including the surrounding polymer layer, possible particle aggregation, and the solvation shell in the liquid medium, whereas FESEM provides the physical size of the dried nanoparticles. Therefore, the larger size range (500 - 700 nm) obtained from DLS is expected and consistent with the nanoscale particle size observed in FESEM images.

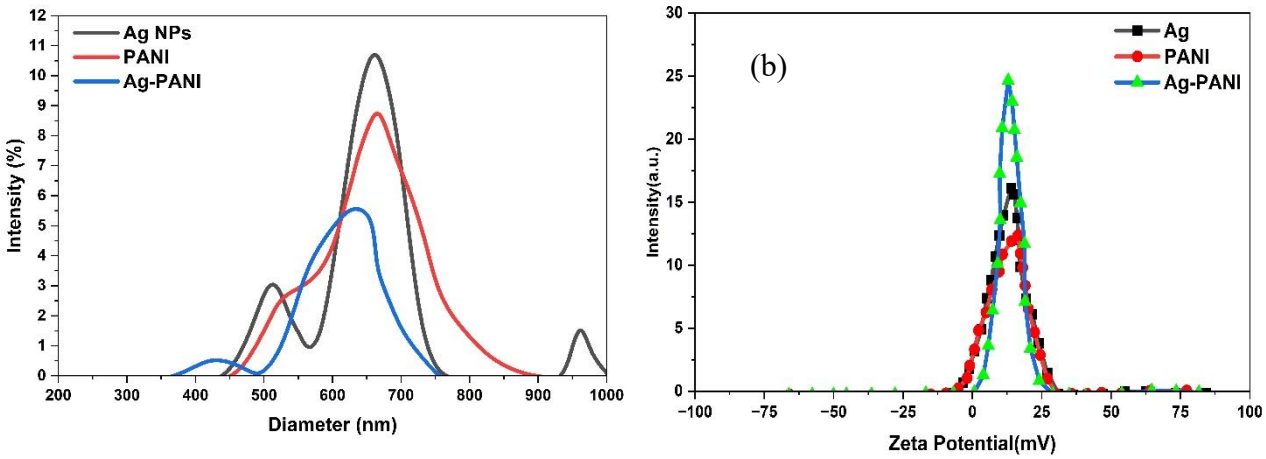

Figure 6 (a) Hydrodynamic particle size distribution obtained by dynamic light scattering (DLS) and (b) zeta potential measurements of Ag nanoparticles, pristine PANI, and the Ag-PANI nanocomposite.

***In vitro* anticancer activity (MTT assay)**

The anticancer activity of the green-synthesized Ag-PANI nanocomposite was evaluated against MCF-7 human breast cancer cells using the MTT assay after 24 h of incubation. Cell viability was determined by measuring the absorbance using a microplate reader and normalizing the values relative to untreated control cells. **Figure 7** illustrates the effect of nanocomposite concentration on cell viability, while **Table 1**

summarizes the corresponding statistical parameters obtained from the experiment [58].

As **Figure 7** indicates, Ag-PANI nanocomposite has a distinct concentration-dependent cytotoxic effect. The cells had a high viability at low concentrations (7.25 and 13.5 µg/mL) suggesting that cytotoxic stress was minimal. Nevertheless, cell viability was gradually diminished with increase in concentration of the nanocomposite and stronger cytotoxic outcomes were recorded at higher concentrations (60 and 100 µg/mL).

Table 1 contains the quantitative data, that is, the mean optical density (O.D.), the standard deviation and the outcomes of the multiple range test that were conducted by Duncan. The gradual reduction of the O.D. values as the concentration of nanocomposite is increasing indicates the inhibition of the cellular metabolic activity. Duncan test of statistical analysis showed significant difference between the experimental concentrations ($p < 0.05$). **Table 1** shows that various letters reflect statistically significant differences between treatments as per the multiple range test as proposed by Duncan ($p < 0.05$), though treatments with the same letter do not significantly differ [59].

Based on the dose–response trend, the half-maximal inhibitory concentration (IC_{50}) of the Ag-PANI nanocomposite was estimated graphically to be approximately 45 µg/mL, indicating a moderate cytotoxic effect against MCF-7 breast cancer cells. In comparison, the reference anticancer drug cisplatin exhibited lower O.D. values, indicating stronger cytotoxic potency. Statistical comparison further confirmed significant differences ($p < 0.05$) between the cytotoxic activity of cisplatin and the Ag-PANI nanocomposite at comparable concentrations.

The cytotoxic effect observed could be due to the synergistic effect between the silver nanoparticles and the polyaniline matrix that could trigger oxidative stress, mitochondrial disturbance and perturbations in the cellular metabolic pathways. Additionally, the conductive property of polyaniline can be useful in electron-transfer mechanisms at the nano- bio interface that encourages redox imbalance and oxidative stress amplification in cancer cells. It is also possible that the contact between the Ag-PANI nanocomposite and cancer cell membranes is increased by the increased colloidal stability and positive surface charge which results in cellular uptake and cytotoxic activity.

Overall, the results presented in **Figure 7** and **Table 1** confirm that the Ag-PANI nanocomposite exhibits significant *in vitro* anticancer activity against MCF-7 cells in a concentration-dependent manner. However, further investigations involving normal cell lines are required to evaluate the selectivity and biosafety of the nanocomposite for potential biomedical applications.

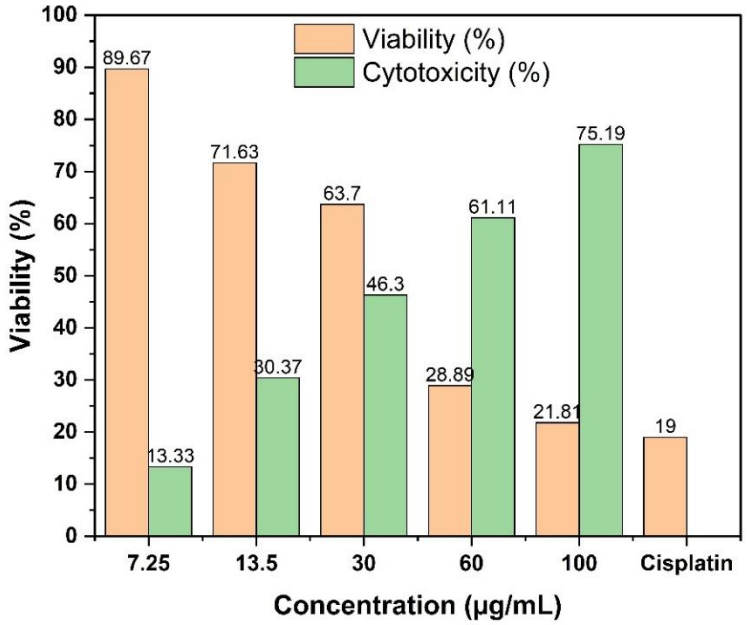

Figure 7 Effect of Ag-PANI nanocomposite concentration on the viability of MCF-7 breast cancer cells determined by the MTT assay after 24 h of incubation.

Table 1 MTT assay-based anticancer activity of Ag-PANI nanocomposite against breast cancer cells.

Concentration (µg/mL)	N	Mean O. D.	Std. Deviation	Duncan Test
7.25	3	0.897	0.018	D
13.5	3	0.716	0.022	C
30	3	0.637	0.019	BC
60	3	0.289	0.015	B
100	3	0.218	0.014	A
Cisplatin (control)	3	0.190	0.012	A

Antioxidant activity of Ag-PANI nanocomposite

Different free radical scavenging tests, including DPPH, hydrogen peroxide (H_2O_2), hydroxyl radical (•OH) and superoxide anion ($^{-}O_2$) were used to determine the antioxidant activity of the Ag-PANI nanocomposite, using vitamin C as a reference antioxidant. The relative scavenging efficiencies are in **Figure 8**.

It is indicated in Figure 8 that the Ag-PANI nanocomposite has significant free radical scavenging ability, which highly depends on the radical type. The nanocomposite has a scavenging activity of 30.7 ± 1.4% in the DPPH assay that is somewhat higher than that of vitamin C (26.2 ± 1.1%), which means that the nanocomposite has an effective ability to donate electrons or hydrogen atoms to stabilize the DPPH radical [60].

The Ag-PANI nanocomposite has a scavenging activity of 47.9 ± 1.6 in the hydrogen peroxide (H_2O_2) scavenging assay, compared to a scavenging assay of 66.8 ± 1.3 of the vitamin C. This fact may be explained by the rapid electron-donating property of vitamin C in aqueous solution that increases its reaction with H_2O_2 over the nanocomposite.

To determine the scavenging of hydroxyl radical (•OH), the Ag-PANI nanocomposite is better than vitamin C with a scavenging capacity of 21.4 ± 1.0% versus 12.6 ± 0.8% of vitamin C. The high surface reactivity of the nanocomposite could be related to the high performance of this catalyst. Conversely, Ag-PANI nanocomposite has a low activity in scavenging superoxide anion (O_2^-) (9.2 ± 0.7%) than vitamin C (33.5 ± 1.2%), which is evidence of greater affinity of the vitamin C to this radical species [61].

It is possible to attribute the antioxidant activity that is observed of the Ag-PANI nanocomposite to its nanoscale dimensions, large surface area, and the existence of bioactive functional groups that are because of the green synthesis pathway. These characteristics improve the processes of electron transfer and offer numerous active sites of radical stabilization. In general, the findings of **Figure 8** suggest that Ag-PANI nanocomposite has significant antioxidant properties and can be considered as a promising nano-antioxidant with radical scavenging ability depending on the concentration [62].

The variation in scavenging efficiency observed for different radicals can be attributed to the distinct reaction mechanisms involved in each assay. Radicals such as DPPH and H_2O_2 are more accessible to electron or hydrogen donation processes occurring on the surface of the nanocomposite, whereas highly reactive radicals such as hydroxyl (•OH) and superoxide (O_2^{-}•) may interact differently depending on their reactivity and diffusion behavior in the reaction medium. The surface-active silver nanoparticles and the functional groups in the PANI matrix are involved in Ag-PANI system, which achieves the radical scavenging process via electron transfer and surface adsorption. All these effects are what accounted to the differences in the antioxidant effectiveness of the radical systems that were tested.

These 2 activities of Ag-PANI nanocomposite as a pro-oxidant and antioxidant can be attributed to the difference in physicochemical environments where these activities take place. The nanocomposite can be used in chemical antioxidant assays, in which the nanocomposite is able to donate electrons or hydrogen atoms to neutralize free radicals and this leads to quantifiable radical scavenging activity of the

nanocomposite. Conversely, in a biological context, e.g. cancer cells, Ag nanoparticles can facilitate the production of intracellular reactive oxygen species (ROS) via cellular interactions and connections in mitochondria. This excess production of ROS is capable of causing oxidative stress and consequent damage of cancer cells. Thus, the visible pro-oxidant and antioxidant actions are explained by various environments of reactions and mechanisms.

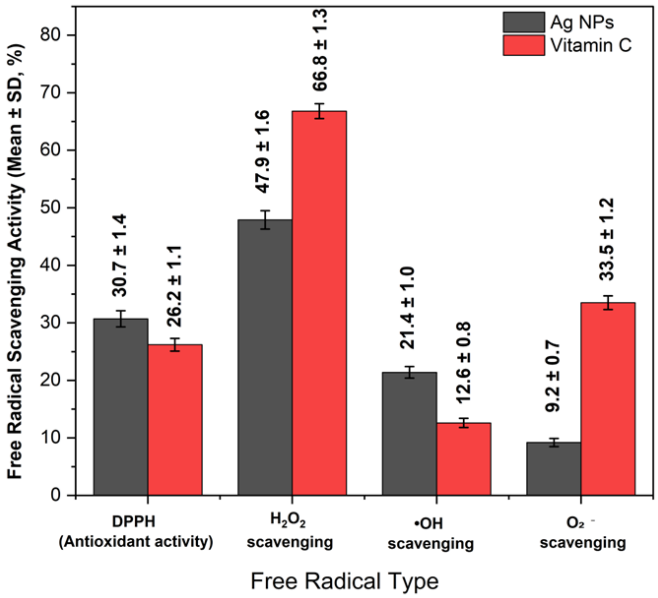

Figure 8 Antioxidant activity of the Ag–PANI nanocomposite evaluated using different radical scavenging assays (DPPH, H_2O_2, hydroxyl, and superoxide radicals) compared with vitamin C as a reference antioxidant.

Antibacterial activity of Ag-PANI nanocomposite

Figure 9 presents the antibacterial activity of the Ag-PANI nanocomposite against Escherichia coli (Gram-negative) and *Staphylococcus aureus* (Gram-positive) at different nanocomposite concentrations ranging from 250 to 1,250 µg/mL. The inhibition zones correspond to the wells labeled from B to F, while region A represents the control sample and was therefore not included in the quantitative analysis [63].

In the case of *E. coli*, the smallest inhibition zone was observed at 250 µg/mL (region B), with a diameter of 5.0 ± 0.07 mm, indicating weak antibacterial activity at low concentration. As the nanocomposite concentration increased, the inhibition zones gradually expanded to 11.0 ± 0.87 mm at 500 µg/mL (region C) and 14.0 ± 0.54 mm at 750 µg/mL (region D). A further increase was observed at 1,000 µg/mL (region E), while the maximum antibacterial activity was recorded at 1,250 µg/mL (region F), where the inhibition zone reached 24.0 ± 0.91 mm.

Similarly, a concentration-dependent antibacterial response was observed for *Staphylococcus aureus*, although the inhibition zones were slightly smaller compared with those of *E. coli*. The inhibition zone diameter increased from 5.0 ± 0.03 mm at 250 µg/mL (region B) to 9.0 ± 0.43 mm at 500 µg/mL (region C) and 12.0 ± 0.68 mm at 750 µg/mL (region D). At 1,000 µg/mL (region E), the inhibition zone reached 15.0 mm, while the highest antibacterial activity was observed at 1,250 µg/mL (region F), with an inhibition zone of 21.0 ± 0.73 mm.

The differences in the antibacterial activity between the *E. coli* and the *S. aureus* can be explained by differences in the cell wall structures of these bacteria. Gram-negative bacteria like *E. coli* have a thinner layer of peptidoglycan hence they tend to interact and penetrate the Ag-PANI nanocomposite better. Gram-positive bacteria including *S. aureus*, on the contrary, possess a thicker peptidoglycan structure and can serve as a more effective barrier to nanoparticles diffusion.

This may be explained by the fact that the improved antibacterial activity at higher concentrations could be a result of the synergistic effect between silver nanoparticles and the PANI matrix. It is probable that this effect is a combination of several different processes, which are release of Ag^{+} ions, interference with the cell membranes of bacteria, inhibition of different enzymes, and increased electrostatic interaction between positively-charged nanoparticles and negatively-charged bacterial cell membranes.

The Ag-PANI nanocomposite was also compared with a standard antibiotic that was used as a positive control on the antibacterial activity. Even though the size of the inhibition zones formed by the nanocomposite tended to be smaller than the size of the inhibition zone formed by antibiotic, the findings indicate that the Ag-PANI composite has a high potential of being used as a substitute antimicrobial material.

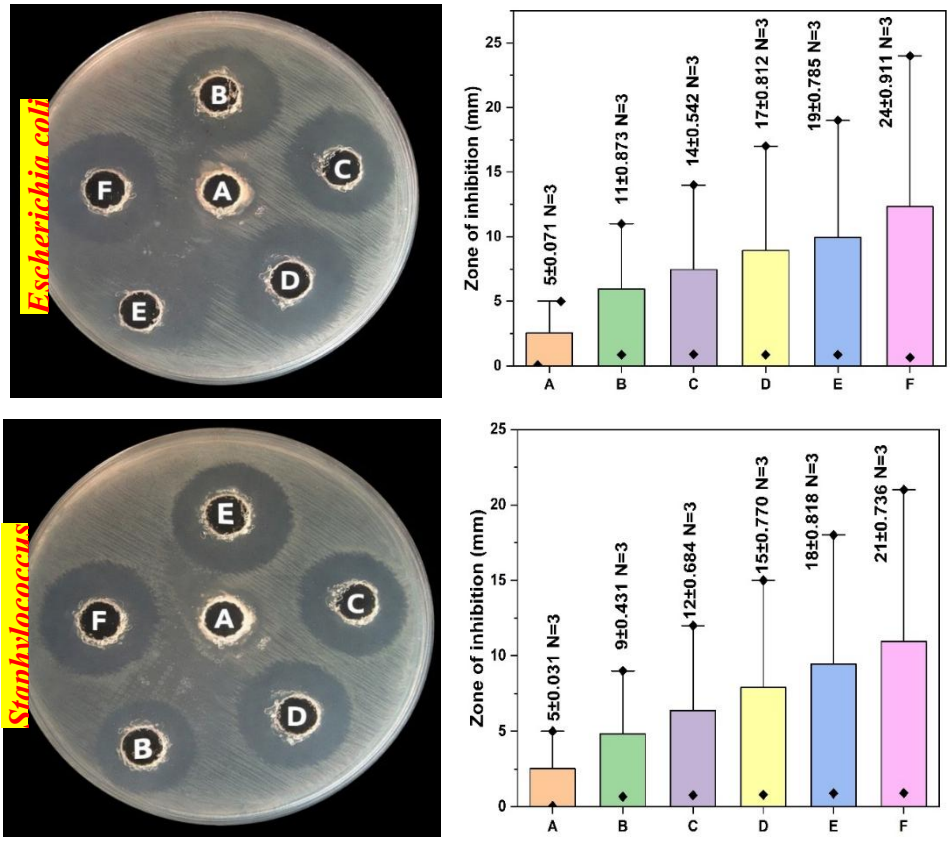

Figure 9 Antibacterial activity of the Ag-PANI nanocomposite against Escherichia coli and Staphylococcus aureus determined by the agar diffusion method at different nanocomposite concentrations.

The Ag-PANI nanocomposite that was prepared in the current study has competitive biological performance because of the interaction between the silver nanoparticles and the conductive polymer matrix in a synergistic manner that is reported to have not been previously reported in Ag-based nanocomposites. As has already been demonstrated in the previous studies, Ag-based polymer nanocomposites tend to have better biological activity than pure Ag nanoparticles due to the fact that the polymer matrix allows to better disperse, stabilize and contact the nanoparticles with the biological systems. As an example, Ag-PANI nanostructures have been also suggested to have high antibacterial properties and a better stability than pure Ag nanoparticles because Ag is stabilized on the polymer network [64]. On the same note, Ag-polymer nanocomposites have displayed enhanced antimicrobial and cytotoxic properties due to controlled release of Ag ions as well as decreased aggregation of nanoparticles in the polymer matrix [65]. In the current article, porous

PANI has been used to provide high porosity and conductive environment, which enables electron transfer and stabilization of Ag nanoparticles, which in combination with the above, promotes anticancer, antioxidant, and antibacterial effect. Such structural and physicochemical properties help to point out the possible benefits of the Ag-PANI nanocomposite as opposed to most traditional Ag nanomaterials.

Conclusions

The Ag-PANI multifunctional nanocomposite was successfully synthesized via a green and environmentally friendly route using *Hibiscus sabdariffa* extract. Structural characterization using XRD and FTIR confirmed the successful formation of crystalline Ag nanoparticles and their incorporation into the polyaniline matrix, while FESEM and EDX analyses revealed homogeneous dispersion of Ag nanoparticles within the porous PANI framework and confirmed the elemental composition of the composite. In addition, zeta potential analysis demonstrated good colloidal stability of the nanocomposite, which is advantageous for biological applications.

The anticancer activity tested based on the MTT assay exhibited a definite concentration-lengthy cytotoxic impact on the breast cancer cells. With a higher concentration of Ag-PANI nanocomposite, cell viability was reduced progressively. It was approximated that the half-maximal inhibitory concentration (IC_{50}) was 45 µg/mL which fact revealed a moderate cytotoxic effect. The cell viability at higher concentrations was reduced to less than 30%, which shows a strong inhibitory property of the nanocomposite on the proliferation of cancer cells.

The antioxidant assessment also established the fact that the Ag-PANI nanocomposite has the radical-scavenging property. Scavenging efficiencies values were found to be 30.7% in DPPH, 47.9% in H_2O_2, 21.4% in hydroxyl radicals, and 9.2% in superoxide radicals, which implies the capability of the composite to counteract reactive oxygen species. Such findings can be explained by active surface sites and functional groups of both polymer matrix and the synthesis process that are mediated by plants.

The antibacterial activity of the Ag-PANI nanocomposite was confirmed against both *Escherichia coli* and *Staphylococcus aureus*. The inhibition zones increased with increasing nanocomposite concentration, reaching maximum values of 24.0 ± 0.91 mm for *E. coli* and 21.0 ± 0.73 mm for *S. aureus* at 1250 µg/mL, demonstrating strong antibacterial performance.

In general, the synergistic effect between the polyaniline matrix and the silver nanoparticles can be considered as the reason of the improved biological performance of the Ag-PANI nanocomposite. As Ag nanoparticles are important in cytotoxic and antibacterial activity, PANI matrix enhances nanoparticle stability, dispersal and contact with biological systems. Hence, the green-synthesized Ag-PANI nanocomposite is a prospective multifunctional nanomaterial that can be used in biomedical applications, but more studies on selectivity to normal cells and *in vivo* functionality are yet to be carried out.

Declaration of generative AI in scientific writing

Generative AI tools were used only to improve the readability, grammar, and language clarity of the manuscript. These tools were applied under full human supervision, and all authors take complete responsibility for the content of this work. No AI systems were used for data generation, analysis, interpretation, or drawing scientific conclusions. AI tools were not listed as authors or co-authors.

CRediT author statement

Rusul Ali Al-Masaoodi: Conceptualization; Methodology; Investigation; Data Curation; Formal Analysis; Writing - Original Draft. **Muhammad Riyadh Alkenany**: Supervision; Project Administration; Resources; Validation; Writing - Review & Editing; Corresponding Author. **Ahmed A. Abdul-Azeez Al-Safar**: Resources; Investigation; Visualization; Data Curation; Writing - Review & Editing. **Noor Ali Abdul Al-Immah Al-Salman**: Methodology; Investigation; Validation; Writing - Review & Editing.

Availability of data and materials

The data supporting the findings of this study are available from the corresponding author upon reasonable request.

References

[1] A Nizam, N Shireen, MR Hasan, J Narang, F Choudhary, A Rizwan, UM Naikoo, U Ahmad, A Kumar and H Farooqi. Harnessing the power of ternary nanocomposites in comprehensive cancer management. *Discover Sensors* 2025; **1(1)**, 26.

[2] M Sharon and AP Dubey. *CNF a cousin of CNT is offering a new arena for nanomedicine studies. In*: R Pisano (Ed.). Nanoscience & nanotechnologies. Springer, Cham, Switzerland, 2025.

[3] D Bouras and M Rasheed. Comparison between CrZO and AlZO thin layers and the effect of doping on the lattice properties of zinc oxide. *Optical and Quantum Electronics* 2022; **54(12)**, 824.

[4] P Kush, P Kumar and R Singh. *Functionalized carbon nanostructures in cancer diagnosis and therapy. In*: A Barhoum and K Deshmukh (Eds.). *Handbook of functionalized carbon nanostructures*. Springer, Cham, Switzerland, 2024.

[5] B Dey, S Kundu and BK Sundara. Polymeric nanostructures revolutionizing cervical cancer: Diagnostics, therapeutics, and theranostics. *BioNanoScience* 2024; **14(4)**, 3906-3933.

[6] P Gong, F Wang, Y Hua, J Ying, J Chen and Y Qiao. Collagenase-mediated extracellular matrix targeting for enhanced drug penetration and therapeutic efficacy in nanoscale delivery systems for cancer therapy. *Journal of Nanobiotechnology* 2025; **23(1)**, 733.

[7] P Chaubisa, D Dharmendra, Y Vyas, P Chundawat, C Paliwal and A Ameta. Biological activity of PANI-tetrazole and PANI-pyrazole composites against microbial strains. *Discover Chemistry* 2025; **2(1)**, 59.

[8] P Kush, P Kumar and R Singh. *Functionalized carbon nanostructures in cancer diagnosis and therapy. In*: A Barhoum and K Deshmukh (Eds.). *Handbook of functionalized carbon nanostructures*. Springer, Cham, Switzerland, 2023.

[9] U Shashikumar, H Goel, I Rana, PC Tsai, KB Manjappa, PV Pham, G Andaluri, KR Ranjan, YC Lin, VK Ponnusamy and PC Huang. Breaking the 'forever' bond: Photocatalytic degradation of per- and polyfluoroalkyl substances using ternary photocatalysts. *Reviews in Environmental Science and Bio/Technology* 2025; **24(3)**, 607-659.

[10] M Rasheed, MM Saleem, TR Marzoog, MM Taki, D Bouras and IA Hashim. Effect of caffeine-loaded silver nanoparticles on minerals concentration and antibacterial activity in rats. *Journal of Advanced Biotechnology and Experimental Therapeutics* 2023; **6(2)**, 495-509.

[11] TM Rashid, MI Rahmah, WK Mahmood, MQ Fahem, MS Jabir, AK Bidan, S Adbalrazaq, MH Jawad, DM Awaid, MA Qamandar and SM Alsaffar. Eco-friendly laser ablation for synthesis of CNF@Au nanoparticles: Insights into enhancing NO_2 gas detection and antibacterial activity. *Plasmonics* 2025; **20(10)**, 8461-8472.

[12] MH Jawad and MR Abdulameer. The effect of background argon gas pressure on parameters of plasma produced by DC glow discharge. *Iraqi Journal of Science* 2023; **64(3)**, 1210-1218.

[13] A Saif, S Ali, S Jamil, T Kamal, MJ Latif, SR Khan, H Arshad, U Mariam and S Liaqat. Comparison of catalytic applications of CaO-Ag bimetallic nanoparticles and its composite: CaO-Ag/Na-alg/PANI. *Journal of Inorganic and Organometallic Polymers and Materials* 2025; **35(5)**, 3344-3365.

[14] HAR Abdullah, MQ Fahem, ZT Turki and MH Jawad. Effect of photothermal therapy using PANI-Fe_2O_3-Cys nanocomposites on breast cancer cells with antibacterial activity and cytotoxicity study. *The European Physical Journal E* 2025; **48(6)**, 40.

[15] AE Dobamo, AA Tsegaye, AM Taddesse, G ShiferaWeldegrum and BA Hussein. Facile synthesis of Ag/PANI/rGO nanocomposite for electrochemical detection of toxic heavy metals in water. *Discover Electrochemistry* 2025; **2(1)**, 42.

[16] MH Jawad, AA Assi and AM Hameed. Hydrothermal synthesis of zinc oxide nanostructures using varied reactor designs: A comparative study. *Plasmonics* 2025; **20(9)**, 7883-7894.

[17] R Jaswal, D Kumar, CH Park and KH Min. Plasmonic nanoparticle-integrated nanofibers: Advancements in nanobiotechnology for biomedical applications. *Journal of*

Pharmaceutical Investigation 2026; **56(2)**, 217-255.

[18] APS Raman, M Aslam, Naina, C Verma, A AlFantazi, P Jain and K Kumari. Composite nanoarchitectonics based on graphene oxide in energy storage and conversion: Status, challenges & opportunities. *Journal of Inorganic and Organometallic Polymers and Materials* 2024; **34(11)**, 5035-5065.

[19] A Chopra, Y Kumari, S Dudeja, R Sharma, AP Singh and R Bhatia. A comprehensive exploration of Chitosan-based nanoparticles for drug delivery and biosensing applications. *Biotechnology for Sustainable Materials* 2025; **2(1)**, 21.

[20] A Aggarwal, D Bose, D Monteiro, K Meyers, N Kapadia and T Asha. Nanomaterials for enhanced detection of some organophosphate and organochlorine pesticides: A comprehensive review of recent advances. *Journal of Nanoparticle Research* 2025; **27(4)**, 92.

[21] M Muniyasamy, R Varatharaj and SKK Kannan. Experimental and DFT investigation on the ultra selective determination of Hg^{2+} ion in water implementing a PAni-RR5B composite modified GCE electrode. *Journal of Inorganic and Organometallic Polymers and Materials* 2025; **35(5)**, 3839-3856.

[22] S Paramshetti, SI Angadi and PV Patil. Conductive polymers and their composites for biomedical applications: A review. *Biomolecules* 2023; **13**, 704.

[23] AH Majeed, LA Mohammed, OG Hammoodi, S Sehgal, MA Alheety, KK Saxena, SA Dadoosh, IK Mohammed, MM Jasim and NU Salmaan. A review on polyaniline: Synthesis, properties, nanocomposites, and electrochemical applications. *International Journal of Polymer Science* 2022; **2022(1)**, 9047554.

[24] MS Horrocks, KE Zhurenkov and J Malmstrom. Conducting polymer hydrogels for biomedical applications. *APL Bioengineering* 2024; **8**, 031503.

[25] AV Shabalina and others. Nanoparticle-polymer composites for antibacterial biomedical applications. *Nanomaterials* 2024; **14**, 1753.

[26] Z Akbari Kheirabadi, Z Nazemi, M Janmohammadi, F Radmanesh, HR Moslemi and MS Nourbakhsh. Biocompatible and antibacterial co-electrospun tragacanth gum and polyaniline nanofibers for skin tissue engineering. *Scientific Reports* 2025; **15(1)**, 38647.

[27] WLV Belino, LC Lieb, JHA Ferreira, DY Tiba, OPL De Souza, TMS Abreu, FWL Silva, RE Santelli, FH Cincotto and T Canevari. Carbon nanomaterial-based sensor for the electrocatalytic detection of water pollutants. *Topics in Catalysis* 2026; **69(1)**, 77-94.

[28] A Abdullahi, T Korumilli and KJ Rao. Revolutionizing food packaging with biobased polymers, active and intelligent materials for enhanced food safety and sustainability. *Food and Bioprocess Technology* 2025; **18(8)**, 6836-6868.

[29] NMA Hadia, MA Sunny, H Hassan, MW Iqbal, NA Ismayilova, S Bibi, M Alzaid, WS Mohamed, MF Hasaneen and A Alanazi. Synergistic performance of PANI@Sn-MOF/Ag (NPs) for next-generation supercapatteries and hydrogen evolution reaction. *Journal of Materials Science: Materials in Electronics* 2025; **36(2)**, 130.

[30] MH Jawad and MR Abdulameer. Eco-friendly laser ablation for synthesis of Al-Ni nanoparticles: Insights into enhancing glucose biosensor performance and antibacterial activity. *Lasers in Manufacturing and Materials Processing* 2026; **13(1)**, 1-22.

[31] MH Jawad and KA Aadim. Plasma jet synthesis of Cu-Zn alloy nanoparticles: Characterization and antibacterial evaluation. *Iranian Journal of Science* 2025. https://doi.org/10.1007/s40995-025-01930-x

[32] IH Ali, RT Kadhim, DFA Alasady, RO Abdulsada and MH Jawad. Green synthesis of CuO nanoparticles and their antibacterial properties. *Theoretical and Experimental Chemistry* 2025; **61**, 148-154.

[33] AS Hussein, FSO Al Jasmi, MH Jawad and MQ Fahem. Fabrication and characterisation of zinc oxide (ZnO) grown on porous silicon (PSi) substrate using different techniques for glucose biosensor. *Silicon* 2026; **18(2)**, 739-750.

[34] AJ Hashim, HM Jaafar, HN Mohsion, MH Jawad, TM Rashid and SM Alsaffar. Hydrothermal synthesis of Ti6O11 nanomaterials for urea

sensing and antibacterial applications. *BioNanoScience* 2025; **15(3)**, 514.

[35] MH Jawad and MR Abdulameer. Study the effect of external voltage on some plasma parameters produced by DC glow xenon gas discharge. *AIP Conference Proceedings* 2024; **2922(1)**, 150003.

[36] MQ Fahem, MH Jawad, RO Abdulsada and ZT Turki. The structure and electrical properties of NiFe2O4 and NiMgFe2O4 prepared via sol-gel method. *Ionics* 2025; **31(6)**, 6475-6481.

[37] B Shakila, SA Alharbi, TA Alahmadi, M Bharathi, SH Hussein-Al-Ali, K Sukumar and MA Munusamy. Study of characterization, antimicrobial, and anticancer potential of albumin-baicalin nanoparticles in Hep3B liver cancer cell lines. *BioNanoScience* 2025; **15(1)**, 180.

[38] A Jalali, IJ Bari and A Salehzadeh. Menthol conjugated magnetic iron oxide nanoparticles induce apoptosis and increase caspase-8 gene expression in gastric cancer cell line. *BioNanoScience* 2024; **14(5)**, 5276-5285.

[39] ZT Turki, MQ Fahem, ZA Mankhi and MH Jawad. Magnetic field effect on cadmium oxide plasma properties detected by laser spectroscopy. *Russian Physics Journal* 2025; **68(5)**, 804-812.

[40] KH Kumar, S Yallappa, M Revanasiddappa, VS Murthy, S Joseph and YT Ravikiran. Ag@PANI/TeO_2 ternary hybrid nanocomposites; Enhanced transport properties and electromagnetic interference shielding performance. *Journal of Materials Science: Materials in Electronics* 2025; **36(19)**, 1161.

[41] T Chen, Y Xiao and G Fang. Light- and temperature-responsive copolymer-MOFs for breast cancer therapy. *Journal of Inorganic and Organometallic Polymers and Materials* 2025; **35**, 2456–2465.

[42] X Liu, S Liu, Q Yang, Y Hu, P Ni, B Ren and G Hu. Novel metal complex-based nanomaterials with excellent fluorescence performance and its treatment on lung cancer cells. *Journal of Inorganic and Organometallic Polymers and Materials* 2024; **34(12)**, 5760-5769.

[43] GIM Mbaz, TC Lebepe, R Maluleke, A Obonai, N Mgedle, OA Aladesuyi, R Kalimutu, T Kodama, A Komiya and SO Oluwafemi. Photothermal depth profiling of gelatin-stabilised gold nanorods-trastuzumab conjugate as a potential breast cancer photothermal agent. *Journal of Inorganic and Organometallic Polymers and Materials* 2024; **34(11)**, 5491-5502.

[44] A Ali, A Madni, N Jan, H Shah, S Khan, A Shafiq, V Torchilin, MI Khan and MA Rahim. Enhanced cytotoxicity of 5-fluorouracil against skin cancer cell lines and 3D spheroid tumor model using solid lipid nanoparticles. *BioNanoScience* 2025; **15(1)**, 31.

[45] M Noruzpour, RA Zakaria, N Zare, S Bourang, HA Ebrahimi and S Granados-Principal. Delivery of *Moringa oleifera* extract via PLA-PEG-FA/chitosan-PLA NPs into breast cancer cell lines. *BioNanoScience* 2025; **15(2)**, 287.

[46] T Abiraamavalli, S Namasivayam, M Lavanya and S Priyanka. Mechanistic insights into the anti-cancer activity of nanosulfur-doped zinc oxide-chitosan-PVA-PEG nanocomposite in MDA-MB-231 triple-negative breast cancer cells. *BioNanoScience* 2025; **15(4)**, 610.

[47] AS Hussein, MQ Fahem, AJ Ghazai, A Ramizy and MH Jawad. Synthesis and characterization of CdS/Polyaniline composites for Rhodamine B and methylene blue dye degradation under visible light. *Journal of Inorganic and Organometallic Polymers and Materials* 2025; **36**, 2099-2110.

[48] MH Jawad and MR Abdulameer. Spectral analysis of brass plasma generated by a Nd: YAQ laser at λ = 1064 nm. *Russian Physics Journal* 2025; **68(6)**, 903-911.

[49] PA Trivedi, JB Naik and PB Patil. Graphene and derivatives for photocatalysis. *Chemical Papers* 2024; **78**, 5705-5722.

[50] R Wang, Z Huang, Y Xiao, T Huang and J Ming. Photothermal therapy of copper incorporated nanomaterials for biomedicine. *Biomaterials Research* 2023; **27(1)**, 121.

[51] MQ Fahema, HN Mohsion, ZT Turki, HAR Abdullah and MH Jawad. Preparation and characterization of SiO_2-enhanced TiO_2 thin films for solar cell applications. *Journal of Ovonic Research* 2025; **21(4)**, 419-430.

[52] T Saidani, M Rasheed, I Alshalal, AA Rashed, MA Sarhan and R Barille. Characterization of thin ITO/Au/ITO sandwich films deposited on glass substrates using DC magnetron sputtering.

Research on Engineering Structures and Materials 2024; **10(2)**, 743-770.

[53] WD Hussain, MH Jawad, SF Khaleel and KA Aadim. Effect of laser energy on the properties of SnO:Cd nanoparticles synthesized via pulsed laser ablation in liquid. *Russian Physics Journal* 2025; **68**, 1750-1757.

[54] N Assoudi, A Chaabani, M Rasheed, I Walha, E Dhahri, T Alawsi, D Bouras and R Barille. Comparative examination of the physical parameters of the sol-gel produced compounds $La_{0.5}Ag_{0.1}Ca_{0.4}MnO_3$ and $La_{0.6}Ca_{0.3}Ag_{0.1}MnO_3$. *Optical and Quantum Electronics* 2022; **54(9)**, 556.

[55] RKM Al-Ziyadi, N Hayati, MR Rezaei and A Es-haghi. Preparation and characterization of chitosan-coated nanostructured lipid carriers (CS-NLC) containing (6)-gingerol and investigating their toxicity against MCF-7 breast cancer cell line. *BioNanoScience* 2024; **14(1)**, 153-163.

[56] FH Santos, DC Ferreira, JR Matheus, AE Fai and FM Pelissari. *Antioxidant activity assays for food packaging materials. In*: C Toni (Ed.). Food packaging materials: Current protocols. Springer, New York, 2024, p. 293-309.

[57] E Kadri, K Dhahri, R Barille and M Rasheed. Novel method for the determination of the optical conductivity and dielectric constant of SiGe thin films using Kato-Adachi dispersion model. *Phase Transitions* 2021; **94(2)**, 65-76.

[58] B Lin and G Huang. The antioxidant activity of shaddock peel polysaccharides. *Scientific Reports* 2025; **15(1)**, 9855.

[59] X Zhao, Y Li, X Tang, S Liu, Q Su, P Hu, X Jin, Y Song, J Wang and Y Yang. A major qualitative trait locus increases antioxidant activity in testaless peanut seeds. *Theoretical and Applied Genetics* 2026; **139(1)**, 19.

[60] Y Wu, Z Ma, L Jia, F Qiao, J Zhu and C Liu. Preparation and characterization of colored Tofu with high antioxidant activity. *Journal of Food Measurement and Characterization* 2025; **19(12)**, 9460-9468.

[61] K Wang, C Wang and C Sun. The antibacterial activity, acute toxicity, and antibacterial mechanism of 2,6-dimethyl-4-aminophenol hydrochloride. *Russian Journal of Bioorganic Chemistry* 2025; **51(5)**, 2142-2151.

[62] T Gong, X Wang and Y Yue. *Antibacterial activity of medicinal mushroom. In*: AS Narayanan and D Dharumadurai (Eds.). Medicinal mushrooms. Humana Press, New York, 2026.

[63] W Alghazzawi. Antibacterial activity of promising nanostructured cesium oxide. *Discover Nano* 2025; **20(1)**, 140.

[64] X Li, SM Robinson and A Gupta. Functionalized silver nanoparticles as potent antimicrobial agents. *ACS Nano* 2011; **5**, 6500-6509.

[65] NK Guimard, N Gomez and CE Schmidt. Conducting polymers in biomedical engineering. *Progress in Polymer Science* 2007; **32(8-9)**, 876-921.